

1 **CALIBRATION AND VALIDATION OF A MACROSCOPIC MULTI-LANE TRAFFIC**
2 **FLOW MODEL USING A DIFFERENTIAL EVOLUTION ALGORITHM**

3
4
5
6 **Kallirroï N. Porfyri**

7 School of Production Engineering and Management,
8 Technical University of Crete,
9 University Campus, Kounoupïdiana, Chania 73100, Crete (Greece)
10 Tel: +30 28210-37383; Email: kporfyri@dssl.tuc.gr

11
12 **Anargiros I. Delis**

13 School of Production Engineering and Management
14 Technical University of Crete,
15 University Campus, Kounoupïdiana, Chania 73100, Crete (Greece)
16 Tel: +30 28210-37751; Email: adelis@science.tuc.gr

17
18 **Ioannis K. Nikolos, Corresponding Author**

19 School of Production Engineering and Management
20 Technical University of Crete,
21 University Campus, Kounoupïdiana, Chania 73100, Crete (Greece)
22 Tel: +30 28210-37300; Email: jnikolo@dpem.tuc.gr

23
24 **Markos Papageorgiou,**

25 School of Production Engineering and Management
26 Technical University of Crete,
27 University Campus, Kounoupïdiana, Chania 73100, Crete (Greece)
28 Tel: +30 28210-37240; Email: markos@dssl.tuc.gr

29
30
31 Word count: 5,490 words text + 8 tables/figures x 250 words (each) = 7,490 words

32
33
34
35
36
37
38 November 7th, 2016

1
2
3
4
5
6
7
8
9
10
11
12
13
14
15
16
17
18
19
20
21
22
23
24
25

ABSTRACT

The calibration and validation of second-order macroscopic traffic flow models constitutes a difficult task; and in fact, relatively few calibration results for such macroscopic traffic flow models have been reported so far. This work evaluates a multi-lane second-order macroscopic gas-kinetic traffic (GKT) flow model and its numerical discretization, using real traffic data from a motorway network in the U.K.; where recurrent congestion originated from high on-ramp flows during the morning peak hours is occurring. In the model, the lane-changing terms, simulating lane-changes due to vehicle interactions as well as spontaneous ones, are introduced as source and sink terms in the model equations. The model provides the ability to use different calibration parameters per lane. A high-order finite volume scheme is implemented for spatial discretization, while time integration is based on a high-order implicit-explicit Runge-Kutta method. A relatively new optimization algorithm, namely a parallel, metamodel-assisted Differential Evolution (DE) algorithm, is employed for the calibration of the model parameters by searching for the global optimal solution. Numerical simulations demonstrate that the proposed model is reasonably accurate in reproducing traffic dynamics in the multi-lane framework, while the DE algorithm can be effectively used for its calibration, as well as for other similar macroscopic models.

Keywords: Macroscopic Traffic Flow Model, Multi-Lane, Calibration, Validation, Differential Evolution Algorithm

1 INTRODUCTION

2 In the last few decades, traffic flow theory, modeling, and simulation have gained considerable
3 attention since overall traffic demand has increased and more data as well as easy access to
4 computing power has become available. Moreover, this growing interest to traffic flow modeling
5 stems also from the need for reliable traffic management, so as to optimize traffic efficiency and
6 safety under various traffic flow conditions. One of the main issues, regarding traffic flow
7 models, is their level of proximity to reality and its representation. Hence, to ensure the validity
8 of any model in performing real-world simulations and provide results that are reliable, the
9 application of calibration and validation processes is deemed mandatory.

10

11 Traffic simulation models can be classified depending on which aspects of traffic modeling one
12 is interested in. Specifically, microscopic simulation models describe traffic flow behavior at a
13 high level of detail, by capturing the behavior of each individual vehicle; while macroscopic
14 approaches represent traffic in lesser detail by using aggregated variables, such as flow, density,
15 and mean speed (*I*). Further, the existence of multiple lanes (with possible lane-drops), on- and
16 off-ramps, and intersections, necessitates the development of proper multi-lane models, which
17 may effectively simulate vehicle lane changes and overtaking maneuvers.

18

19 No matter which approach is used, accurate modeling of traffic flow requires three types of data:
20 model inputs, model parameters and observed outputs. Model inputs involve the demand-side
21 data, for which a traffic simulation is performed. Model parameters involve different types of
22 supply-side parameters used in the traffic simulation, depending on the level of complexity in
23 modeling. This is true for both microscopic and macroscopic models, since they all contain in
24 their structure some set of parameters, whose values represent the particular road network's
25 traffic flow features. The output data observed in real-world is required to compare model
26 outputs and evaluate the accuracy of the models. Macroscopic models call for a relatively small
27 number of parameters, compared to microscopic ones, which results in significantly less
28 demanding and computationally expensive, but by no means trivial, calibration, and validation
29 processes and, therefore, in a more versatile model development for real-world applications.

30

31 Macroscopic traffic flow models, depending on the number of differential equations they
32 involve, can be categorized as first-, second- or higher-order models. The approaches of the class
33 of first-order models, originally developed by Lighthill–Whitham–Richards (LWR model) (2),
34 consist of the continuity equation to represent the evolution of traffic density. However, these
35 models suffer from several limitations and they prove inadequate to describe complicated
36 dynamics of traffic flow; in particular, they do not allow for variations of speed around the
37 equilibrium fundamental diagram and they fail to replicate some non-linear phenomena observed
38 in real traffic, such as the hysteresis and capacity drop, the stop-and-go waves at bottlenecks, as
39 well as the diffusion of traffic platoons. The second- or higher-order models, with the pioneering,
40 among them, Payne model (3), utilize an additional evolution equation, the momentum one, to
41 describe flow/speed dynamics. Although such models have the potential to reproduce the above-
42 mentioned non-linear phenomena with higher accuracy when compared with real traffic data,
43 they include a higher number of parameters; and small changes to them may result in quite
44 different predictions; consequently, they call for a complex but compulsory calibration process to
45 enhance their prediction accuracy.

46

47 As pointed out in (4) and (5), the validation process is the ultimate criterion for assessing the
48 accuracy of representing real traffic phenomena, and hence the usefulness of an existing or new

1 macroscopic traffic flow model as a practical tool for efficiently simulating and optimizing
 2 traffic flow for specific infrastructures. Compared to microscopic models, relatively few works,
 3 which also include methods for solving the involved parameter estimation problem, are available
 4 for the calibration and validation process of macroscopic models. Employed algorithms include
 5 the deterministic complex algorithm of Box in (6-10), the deterministic Nelder-Mead algorithm
 6 employed in (11, 12), the genetic algorithm in (13, 14), the stochastic cross-entropy method
 7 utilized in (15), and stochastic collocation in (16). It is important to note here that, in terms of
 8 validating macroscopic multi-lane or lane-changing models, very few works exist, and these
 9 usually involve first-order models, we refer for example to (17). To the best of our knowledge,
 10 there are virtually no published works involving the calibration and validation of second-order
 11 multi-lane macroscopic models. This is probably due to the complexity involved in the
 12 modeling but also to the increased number of parameters that need to be calibrated.
 13 Furthermore, as it was pointed out in (15), different combinations of the set of parameters may
 14 result in a large number of local optima, hence classical gradient-based methods may not be
 15 effective.

16
 17 The goal of the present study is to validate a recently presented (single-class) multi-lane second-
 18 order gas-kinetic traffic flow (GKT) model (18) with respect to its accuracy in the reproduction
 19 of the congestion created at freeways close to on/off-ramps, using real traffic data from a three-
 20 lane freeway stretch in the U.K. Both interactive and spontaneous lane changes are explicitly
 21 taken into account by the proposed multi-lane model, which aims to describe the behavior of
 22 driver-vehicle units regarding overtaking, deceleration/acceleration, and lane changing
 23 maneuvers. A high-resolution relaxation finite-volume scheme is utilized for the numerical
 24 approximation, in space and time, of the underlying partial differential equations (19), which
 25 constitutes an essential ingredient in the simulation process as well as in the calibration and
 26 validation procedures. The optimization method employed is a recently developed parallel
 27 surrogate-model-assisted Differential Evolution algorithm (20, 21). We emphasize that this
 28 optimization algorithm is applied for the first time for the calibration purposes of a second-order
 29 multi-lane macroscopic traffic flow model, where its parameter estimation constitutes a hard
 30 (constrained) continuous multi-extremal optimization problem.

31 THE MULTI-LANE GKT MODEL

32 In this section, we briefly present the multi-lane second-order GKT model, recently developed in
 33 (18). In general, continuous models that simulate multi-lane traffic flow dynamics, are based on a
 34 nonlinear system of conservation laws with additional source/sink terms, in order to take into
 35 account lane-changes due to vehicle interactions, as well as spontaneous ones. Hence, assuming
 36 a highway with N lanes, which are numbered by $l = 1, 2, \dots, N$, the multi-lane GKT model can
 37 be written in vector form (for each lane, l), supplied with initial conditions, as follows
 38
 39

$$\partial_t \mathbf{u}_l + \partial_x \mathbf{f}(\mathbf{u}_l) = \mathbf{s}(\mathbf{u}_l) + \mathbf{w}_l(\mathbf{u}_1, \dots, \mathbf{u}_N), \quad (1)$$

$$\mathbf{u}_l(x, 0) = \mathbf{u}_{l,0}(x),$$

40
 41 where the functions \mathbf{u}_l , $\mathbf{f}(\mathbf{u}_l)$ and $\mathbf{s}(\mathbf{u}_l) \in \mathbb{R}^2$ with $\mathbf{u}_l = [u_l^1, u_l^2]^T = [\rho_l, q_l]^T$, $\mathbf{f}(\mathbf{u}_l) =$
 42 $[\rho_l u_l, \rho_l u_l^2 + \theta_l \rho_l]^T$ and $\mathbf{s}(\mathbf{u}_l) = [r_{rmp,1}, (\rho_l V_e^* - \rho_l u_l)/\tau + h_{rmp,1}]^T$. The variables ρ_l and u_l
 43 are the traffic density (number of vehicles per unit length) and the average speed of vehicles at
 44 the l -th lane, for $l = 1, 2, \dots, N$, respectively, whereas q_l is the traffic flow rate (number of

1 vehicles per unit of time), given as $q_l = \rho_l u_l$; the pressure-like term θ_l is a density-dependent
 2 fraction $A(\rho_l)$ of the squared velocity $\theta_l = A(\rho_l)u_l^2$, where $A(\rho_l)$ is given by the Fermi
 3 function as
 4

$$A(\rho_l) = A_{0,l} + \delta A_l \left[1 + \tanh \left(\frac{\rho_l - \rho_{cr,l}}{\delta \rho_l} \right) \right], \quad (2)$$

5
 6 in which $\rho_{cr,l}$ is the critical density in the l -th lane, reflecting the boundary for the transition
 7 from the free flow to congested traffic, with $A_{0,l}$ and $A_{0,l} + 2\delta A_l$ the variance pre-factors
 8 between the aforementioned two states, while $\delta \rho_l$ is the width of the transition region. Typical
 9 ranges of values for the constant parameters $A_{0,l}$, δA_l , and $\delta \rho_l$, along with other typical used
 10 model parameters for the GKT model can be found in (19).
 11

12 Furthermore, terms $r_{rmp,1}$ and $h_{rmp,1}$ reflect the impact of traffic flow from on-ramps (or to off-
 13 ramps) on the first lane and take non-zero values only for the corresponding lane. Specifically,
 14 the term $r_{rmp,1}$ denotes the effective source density that is only active within the merging
 15 (diverging) sections with length l_{rmp} and inflow $q_{rmp,1} > 0$ from (or outflow $q_{rmp,1} < 0$ to) the
 16 ramps, determined as
 17

$$r_{rmp,1}(x, t) = \begin{cases} \frac{q_{rmp,1}(t)}{l_{rmp}} & \text{if } x \text{ inside the merging zone,} \\ 0 & \text{elsewhere,} \end{cases} \quad (3)$$

18
 19 while the term $h_{rmp,1}$ describes changes of the macroscopic local speed by assuming that on-
 20 ramp vehicles merge to the main road at speed $u_{rmp} < u$. On the contrary, the drivers considered
 21 to leave the main road reduce their speed to u_{rmp} before they diverge to the off-ramp. Hence,
 22 this term can be expressed as
 23

$$h_{rmp,1}(x, t) = \frac{q_1 \cdot r_{rmp,1}}{\rho_1} + \frac{(u_{rmp} - u_1) |q_{rmp,1}|}{l_{rmp}}. \quad (4)$$

24
 25 The model also includes a traffic relaxation term that maintains the concentration of velocity in
 26 equilibrium state, with $V_e^*(\rho_l, u_l, \rho_{\alpha,l}, u_{\alpha,l})$ being the dynamic equilibrium speed, with relaxation
 27 time τ , depending not only on the local density ρ_l and mean speed u_l , but also on the non-local
 28 traffic state $(\rho_{\alpha,l}, u_{\alpha,l})$. Thus, the non-local and dynamic equilibrium speed, toward which the
 29 average speed relaxes, is determined as
 30

$$V_e^* = u_{max,l} \left[1 - \frac{\theta_l + \theta_{\alpha,l}}{2A(\rho_{max,l})} \left(\frac{\rho_{\alpha,l} T_l}{1 - \rho_{\alpha,l}/\rho_{max,l}} \right)^2 B(\delta u_l) \right]. \quad (5)$$

31
 32 According to Equation (5), the dynamic equilibrium speed is given by the maximum desired
 33 speed, denoted as $u_{max,l}$, reduced by a braking non-local term in response to necessary
 34 deceleration maneuvers in traffic flow at the downstream interaction location $x_{\alpha,l} = x_l +$

1 $\gamma_l(1/\rho_{max,l} + T_l \cdot u_l)$, with T_l being the desired time gap, $\rho_{max,l}$ the maximum density and γ_l a
 2 scale factor. Finally, $B(\delta u_l)$ is a so-called Boltzmann factor that contains the standard normal
 3 distribution and the Gaussian error function, given as

$$4 \quad B(\delta u_l) = 2 \left[\delta u_l \frac{e^{-\delta u_l^2/2}}{\sqrt{2\pi}} + (1 + \delta u_l^2) \int_{-\infty}^{\delta u_l} \frac{e^{-y^2/2}}{\sqrt{2\pi}} dy \right]. \quad (6)$$

5
 6 This term describes the dependence of the braking interaction on the dimensionless velocity
 7 difference $\delta u_l = (u_l - u_{\alpha,l})/\sqrt{\theta_l + \theta_{\alpha,l}}$, taking into account the velocity and variance at the
 8 actual location x_l and the interaction location $x_{\alpha,l}$, respectively.

9
 10 Further, according to model Equations (1) for the multi-lane traffic, the source term
 11 $\mathbf{w}_l(\mathbf{u}_1, \dots, \mathbf{u}_N) \in \mathbb{R}^2$ represents the sources and sinks due to lane-changing, resulting in a weakly
 12 coupled system of $2N$ equations (18). The components of the lane-changing terms are defined as

$$13 \quad w_l^{1,2} = \left(\frac{1}{T_{l-1}^L} u_{l-1}^{1,2} - \frac{1}{T_l^R} u_l^{1,2} \right) (1 - \delta_{l1}) + \left(\frac{1}{T_{l+1}^R} u_{l+1}^{1,2} - \frac{1}{T_l^L} u_l^{1,2} \right) (1 - \delta_{lN}), \quad (7)$$

14
 15 with $\frac{1}{T_l^L}$ and $\frac{1}{T_l^R}$ being the lane changing rates from lane l to left $l + 1$ and right $l - 1$,
 16 respectively, and δ_{ij} the Kronecker delta. The lane changing rates are defined as

$$17 \quad \frac{1}{T_l^L} = P_L(\rho_{l+1})v(\rho_l) + S_l^L \quad (8)$$

$$18 \quad \frac{1}{T_l^R} = P_R(\rho_{l-1})(1 - P_L(\rho_{l+1}))v(\rho_l) + S_l^R,$$

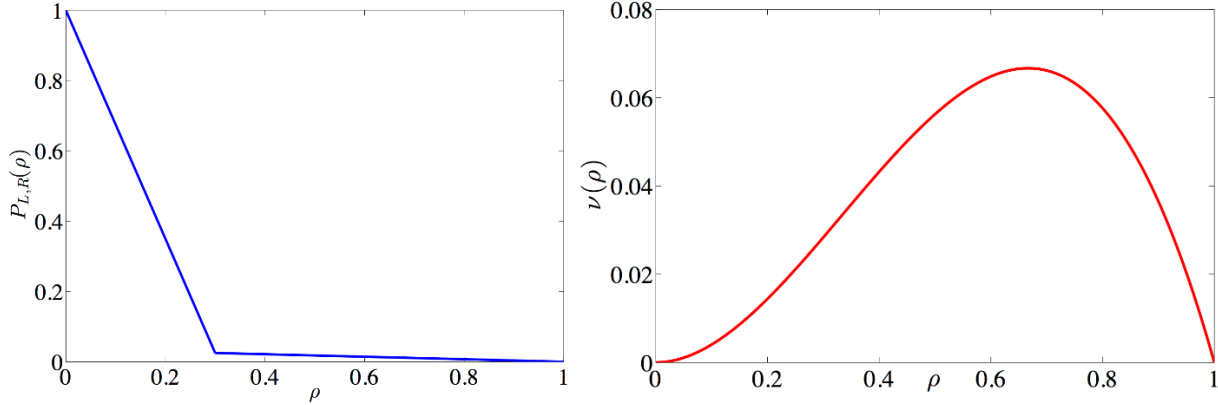
19 where the terms $P_{R,L}(\rho_l)$ are the lane-changing probabilities in response to vehicle interactions
 20 and $v(\rho_l) = v_f(1 - \rho_l)\rho_l^2$ are the interaction frequencies regarding deceleration and
 21 acceleration; for simplicity, considered that $P_R(\rho) = P_L(\rho)$. The shape of $P_{R,L}(\rho_l)$ depends on a
 22 characteristic density value (ρ_p), while that of $v(\rho_l)$ depends on the value of v_f , as depicted for
 23 example in Figure 1.

24
 25 Further, we assume here that the spontaneous lane changes, which are not caused by vehicle
 26 interactions and described by the terms $S_l^{L,R}$, are formulated as

$$27 \quad S_l^{L,R} = k_l^{L,R} \left(1 - \frac{\rho_{l\pm 1}}{\rho_{max,l\pm 1}} \right)^\beta \quad (9)$$

28
 29 in which $k_l^{L,R}$ and β are spontaneous lane-changing parameters (18). For the spontaneous lane-
 30 changing terms in Equation (9), we adopt the European-rule of primarily using the right lane at
 31 low densities (22, 23). Calibration results have shown that spontaneous lane-changing influences
 32 mainly low-density regimes. Setting $\beta = 8$ in Equation (9), a smooth correction pre-factor G_{Eu} ,

1 with $0 < G_{Eu}(\rho) < 1$, is used to account for the European traffic rule by modifying S_l^L as $S_l^L G_{Eu}$
 2 and S_l^R as S_l^R / G_{Eu} (18). Furthermore, the probability function considered for lane-changing
 3 maneuvers can be considered as realistic and in-line with previous works in the literature (24).
 4



5
 6 **FIGURE 1 (Left) Lane changing probability for $\rho_{cr,l} = 0.3\rho_{max,l}$ and $\rho_P = 0.025$. (Right)**
 7 **Lane changing frequency for normalized density, for $\nu_f = 0.45$.**

8
 9 To numerically approximate the multi-lane GKT model, we apply a higher-order finite-volume
 10 relaxation scheme. The spatial discretization is based on a fifth-order Weighted Essential Non-
 11 Oscillatory-type (WENO) finite volume scheme, while time integration is based on a third-order
 12 implicit-explicit (IMEX) Runge-Kutta method. The numerical scheme is stable under the usual
 13 Courant-Friedrichs-Lewy (CFL) stability condition for explicit discretization schemes. The
 14 accuracy, simplicity and robustness of this higher-order scheme, compared to low-order ones, for
 15 simulation of various traffic flow models has been recently demonstrated in (19), where all the
 16 details of the numerical scheme can be found.

17 18 MODEL CALIBRATION

19 Despite their popularity and usefulness, the credibility of macroscopic simulation models depends
 20 greatly on their capability of reproducing with the highest possible level of accuracy their real-
 21 world counterpart. Indeed, the model parameter calibration constitutes a necessary and integral
 22 part of the overall development of any traffic flow model, given the fact that they are for the most
 23 part empirical. However, the estimation of proper values for the unknown model parameters is a
 24 major challenge, because of the highly non-linear nature of the model equations.

25
 26 In this work, we present an automated calibration process for the GKT model parameter vector
 27 for a three-lane freeway stretch. Specifically, the parameter vector to be calibrated is $\mathbf{X} =$
 28 $[u_{max,l}, \rho_{max,l}, \rho_{cr,l}, T_l, \gamma_l, \tau_l, A_{0,l}, \delta A_l, \delta \rho_l, (u_{rmp}/u_1), \nu_f, \rho_P, k_1^L, k_2^R, k_2^L, k_3^R], l = 1, 2, 3$, (34
 29 parameters/design variables in total), which need to be fixed so as to minimize the deviation
 30 between the simulated and observed traffic data reflected via an appropriate cost function,
 31 hereafter denoted by $f(\mathbf{X})$. The proposed model allows for different parameter values to be
 32 introduced for each lane, in order to describe the different dynamics of each lane. Hence, the
 33 calibration of the extended second-order GKT model able to simulate multi-lane traffic flow
 34 dynamics becomes a problem of finding an optimal parameter vector \mathbf{X} subject to model (1) for
 35 all $\mathbf{X} \in \Omega$, where Ω is a constrained admissible region of the parameter space, determined on the
 36 basis of physical constraints. Such a calibration process is a quite complex problem, since it

1 takes the form of minimizing a continuous multi-extrema cost function, which exhibits numerous
 2 local minima, which traditional gradient-based algorithms are likely to fail to avoid. In this work,
 3 a recently developed parallel Differential Evolution algorithm has been applied in order to deal
 4 with the aforementioned complex continuous optimization problem with numerous local minima,
 5 and a relatively large number of design variables.

7 **Metamodel-assisted Differential Evolution (DE) algorithm**

8 Since early in their development, Evolutionary Algorithms (EAs) have become increasingly
 9 attractive across various optimization problems, as a flexible and robust optimization technique
 10 capable of addressing real-world applications, containing multiple objectives and high
 11 dimensional search spaces; however, such algorithms call for significantly increased
 12 computation time requirements. A remedy to this shortcoming appears to be the use of surrogate
 13 models (metamodels), in conjunction with parallel processing. In what follows, we will briefly
 14 present the basic elements constituting a classic DE algorithm, as introduced in (20, 21).

15
 16 The minimization problem is defined as

$$17 \quad \min f(\mathbf{X}) = f(x_1, x_2, \dots, x_n) \quad (10)$$

18 where $f(\mathbf{X}): \mathbb{R}^n \rightarrow \mathbb{R}$ is the cost function to be minimized by modulating the values of the n -
 19 dimensional vector of design variables \mathbf{X} , $x_i \in \mathbb{R}$. During the optimization process, each design
 20 variable x_i is bounded between pre-specified upper and lower values, with superscripts (U) and
 21 (L), respectively

$$22 \quad x_i^{(L)} \leq x_i \leq x_i^{(U)}, i = 1, \dots, n. \quad (11)$$

23
 24 At first, the population is randomly initialized within the given boundaries as:

$$25 \quad x_{k,i}^{(0)} = r \cdot (x_i^{(U)} - x_i^{(L)}) + x_i^{(L)}, \quad k = 1, \dots, N_p, \quad i = 1, \dots, n, \quad (12)$$

26
 27 in which r is a random generated number with uniform probability distribution within the range
 28 $[0, 1]$ and N_p is the (constant) number of individuals (chromosomes) in the population.

29
 30 Subsequently, the differential mutation process is activated, where a new chromosome is
 31 randomly generated for each individual of the current generation. Specifically, the formation of
 32 the new chromosome is based on a triplet of different randomly selected individuals and realized
 33 by adding a weighted difference among the two individuals of the triad to the third one (donor).
 34 Thereafter, the crossover recombination is applied among the perturbed individual and the
 35 current population member (parent), thereby generating the final candidate solution

$$36 \quad x'_{k,i}{}^{(G+1)} = \begin{cases} x_{C_{k,i}}^{(G)} + F \cdot (x_{A_{k,i}}^{(G)} - x_{B_{k,i}}^{(G)}) & \text{if } (r \leq C_r \vee i = i^*), \quad i = 1, \dots, n \\ x_{k,i}^{(G)} & \text{otherwise,} \quad i = 1, \dots, n \end{cases} \quad (13)$$

1 where $x_{C_k,i}^{(G)}$ is the “donor” and (G) is the current generation. The randomly selected integer i^* is
 2 chosen once for all members of the population within the interval $[1, n]$, while the DE control
 3 parameters $F \in [0,1]$ and $C_r \in [0,1]$ for the mutation and crossover operations, respectively,
 4 remain constant during the search process and affect the convergence behavior and robustness of
 5 the algorithm. Subsequently, the selection process takes place to determine which of the parent or
 6 the offspring will survive to the next generation. Therefore, each trial vector $\mathbf{X}'_k^{(G+1)}$ competes
 7 against its counterpart (parent) in the current population $\mathbf{X}_k^{(G)}$ by using a one-by-one comparison.
 8 If the candidate is better fitted than the corresponding current one, it moves to the next
 9 generation, ensuring in this way the survival of the elitists. The DE selection scheme can be
 10 represented as follows for a minimization problem:
 11

$$\mathbf{X}_k^{(G+1)} = \begin{cases} \mathbf{X}'_k^{(G+1)} & \text{if } f(\mathbf{X}'_k^{(G+1)}) \leq f(\mathbf{X}_k^{(G)}), \\ \mathbf{X}_k^{(G)} & \text{otherwise.} \end{cases} \quad (14)$$

12
 13 The application of a classical DE algorithm to realistic computational problems is a time
 14 consuming task, as it requires a significant number of evaluations to achieve an adequate-quality
 15 solution. Thus, to reduce the running time of the algorithm, two strategies have been
 16 incorporated. A surrogate-assisted methodology was utilized to substitute some of the
 17 computationally intensive exact evaluations of trial vectors with low-cost approximations,
 18 without compromising the robustness and the convergence of the DE algorithm. Hence, the DE
 19 algorithm was combined with two Artificial Neural Networks (ANN's), a Multi-Layer
 20 Perceptron (MLP) and a Radial Basis Functions Network (RBFN), which serve as surrogate
 21 models.

22
 23 In each generation of the DE, both surrogate models are re-trained, retrieving their training set
 24 from a database, fed with the previous results of the evaluation procedure; the most promising
 25 individuals from this database are used in each generation for retraining the surrogate models. A
 26 testing set is also retrieved from the database to evaluate in each generation the effectiveness of
 27 both surrogate models and select the most accurate one for use in the current generation. Each
 28 candidate solution is first pre-evaluated with the most accurate surrogate model and compared to
 29 its parent. If the candidate is pre-evaluated as better-fitted, an exact evaluation subsequently
 30 takes place, followed by a second (accurate) comparison with its parent, providing the final
 31 decision on which individual will proceed to the next generation. On the contrary, if the
 32 candidate is pre-evaluated as worse-fitted, compared to its parent, it is abandoned and no exact
 33 evaluation is further needed. In this way, all members in each generation have been selected
 34 through an exact evaluation and selection procedure, while the pre-evaluation, using the
 35 surrogate models, is utilized for removing the likely less promising candidates, with insignificant
 36 computational cost. This technique reduces the computational cost, through the reduction of the
 37 (costly) exact evaluations, without affecting the robustness of the optimization procedure.
 38

39 Moreover, parallel processing was incorporated, using MPI (Message Passing Interface) and
 40 based on the idea of “external-coupling” of the DE with the exact cost function evaluation,
 41 enabling the cooperation with different analysis software in the form of executables (in our case
 42 the macroscopic traffic flow model simulation, followed by the cost function computation). A
 43 detailed description of the utilized parallel surrogate-assisted DE algorithm is presented in (20,

1 2l).

2

3 **Cost function formulation**

4 As already mentioned, the parameter calibration problem addressed here aims at the
 5 minimization of the discrepancy between the simulation results from the multi-lane GKT model
 6 and the observed traffic data collected for the considered network. Specifically, the model is fed
 7 with real measured boundary data (25) to reproduce the complete traffic state. The resulting
 8 model accuracy is evaluated using as cost function a combined total mean square normalized
 9 error of the model-calculated and observed speed and flow

10

$$f(\mathbf{X}) = \frac{1}{C} \sum_{l=1}^N \sum_{k=1}^K \sum_{i=1}^n \left[(1 - \mu) \left(1 - \frac{u_{l,i,k}}{u_{l,i,k}^d} \right)^2 + \mu \left(1 - \frac{q_{l,i,k}}{q_{l,i,k}^d} \right)^2 \right] \quad (15)$$

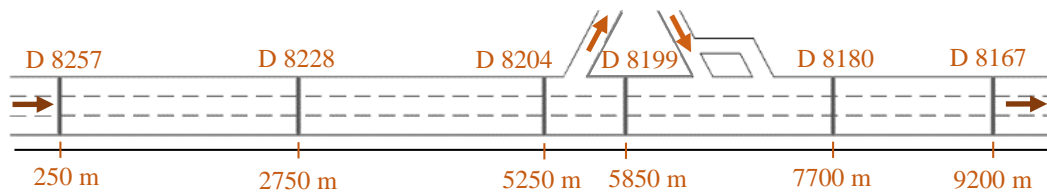
11

12 where, $u_{l,i,k}$, and $q_{l,i,k}$ represent the predicted mean speed and flow, respectively, computed for
 13 lane l , location k (K is the number of detectors that are available for calibration) and time instant
 14 i (n is the simulation time horizon); $u_{l,i,k}^d$ and $q_{l,i,k}^d$ represent, respectively, the observed mean
 15 speed and flow computed at lane l , location k and time instant i , while $C = N \cdot n \cdot K$, and μ is a
 16 weighting factor equal to 0.5.

17

18 The calibration process begins with the generation of an initial population; every chromosome
 19 (design variables vector) is randomly initialized, based on the upper and lower bounds of the
 20 design variables. Subsequently, at each generation the candidate chromosomes are evaluated
 21 according to their cost functions' values, i.e. the deviation between the simulated and the real
 22 traffic data; note that it is this stage that suffers from excessive computational requirements, and
 23 calls for the use of surrogate models. The contribution of these models lies in time-savings, due
 24 to avoiding the "expensive" exact evaluations of all candidate solutions, by using instead a
 25 trained neural network (20), as it was previously described. Then, for each generation, the
 26 reproduction scheme of the DE algorithm generates a new population based on the mutation,
 27 crossover, and selection operators, aiming to new candidate parameter vectors with better cost
 28 function values. The whole procedure is repeated for a pre-described number of generations.

29



30
31

32 **FIGURE 2 A graphical representation of the U.K. freeway stretch considered.**

33

34 **TEST NETWORK AND TRAFFIC DATA**

35 The multi-lane GKT model described previously is applied to a particular motorway network in
 36 the United Kingdom to calibrate its parameters under recurrent traffic flow conditions.
 37 Specifically, the considered network, sketched in Figure 2, is a 9.45 km long freeway stretch
 38 composed of three lanes, and is part of the M56 motorway with direction from Chester to
 39 Manchester. The freeway consists of one off-ramp and a two-lane on-ramp, which, before

merging into the mainstream, splits into two separate lanes. Figure 2 also illustrates the location of the on-ramps and off-ramp, as well as the locations of the available detector stations.

The real-time traffic data, provided by MIDAS database (25), retrieved from 6 detectors (Figure 2), deliver measurements of speed and flow per lane with a time resolution of 60 s; detector stations are also installed on the on-ramps and off-ramp, measuring the ingoing and outgoing flow, respectively. Measured data corresponding to the stretch's boundaries are also available. Performing a qualitative analysis of real-time traffic data, a recurrent congestion, originated from high on-ramp flows during the morning rush hours, is observed. Indeed, by visual inspection of the contour plots shown in Figure 3 (upper) and Figure 5 (upper), which display the space-time evolution of the real speed measurements for the 3rd and 24th of June 2014, respectively, it can be observed that traffic congestion is formed upstream of the second on-ramp between 7–8 a.m. for both days. This congestion propagates upstream, creating an intensive low-speed area of several kilometers on the freeway mainstream.

CALIBRATION AND VALIDATION RESULTS

The numerically discretized multi-lane GKT model is first calibrated to specify the optimal parameter values for the considered network, using the measured data for a specific day. Eventually, in order to demonstrate the validity of the developed model to reliably reproduce the traffic conditions of the examined site, the optimal parameters resulting from the calibration procedure are applied to the same freeway for a different day.

TABLE 1 Range of the parameter vector used for the multi-lane GKT model calibration

| Model parameters | Units | Bounds |
|---|--------------|---------------|
| Desired free speed, $u_{max,l}$ | km/h | [80, 140] |
| Maximum density, $\rho_{max,l}$ | veh/km | [140, 160] |
| Critical density, $\rho_{cr,l}$ | veh/km | [30, 60] |
| Desired time gap, T_l | s | [1, 2] |
| Anticipation factor, γ_l | | [1, 1.5] |
| Relaxation time, τ_l | s | [20, 40] |
| Variance pre-factor for free traffic, $A_{0,l}$ | | [0.006, 0.01] |
| Pre-factor, δA_l | | [0.008, 0.04] |
| Transition width, $\delta\rho_l$ | veh/km | [3.5, 20] |
| Frequency factor for lane changing, ν_f | | [0.1, 1] |
| Critical density for lane changing probability, ρ_p | | [0.02, 0.04] |
| Percentage of reducing speed at exiting/entering, (u_{rmp}/u_1) | | [0.4, 0.9] |
| Spontaneous lane-changing factor, k_1^L | Events/sec/m | [0.001, 0.1] |
| Spontaneous lane-changing factor, k_2^R | Events/sec/m | [0.001, 0.04] |
| Spontaneous lane-changing factor, k_2^L | Events/sec/m | [0.001, 0.1] |
| Spontaneous lane-changing factor, k_3^R | Events/sec/m | [0.001, 0.04] |

Calibration results

The real measurements used in this section were collected on the M56 motorway in U.K. on the 3rd of June, 2014. The multi-lane GKT model parameters, with their corresponding admissible bounds, being consistent with those given in (19), are presented in Table 1. The DE algorithm was employed with a population size equal to 60, whereas the maximum number of generations

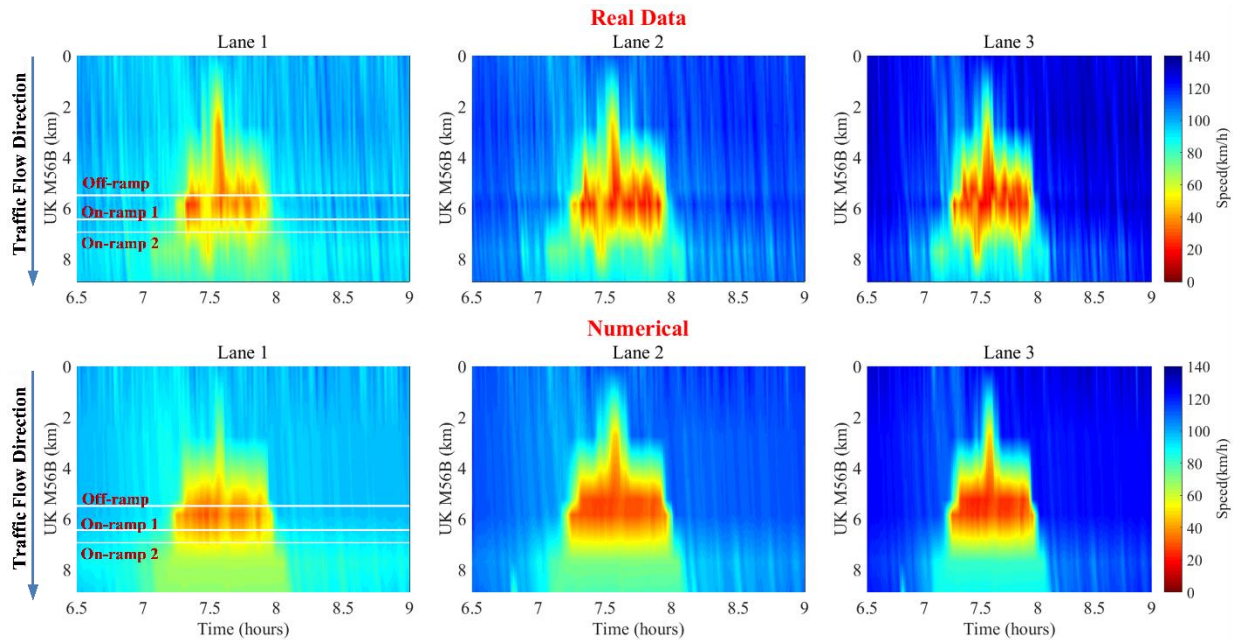
1 was set equal to 1500; the control parameters for the mutation and crossover operations were
 2 $F = 0.6$ and $C_r = 0.45$.

3
 4 The considered 9.45 km stretch was simulated for 2:30 morning peak hours (i.e. from 6:30 a.m.
 5 to 9 a.m.), whereas the space discretization was $\Delta x = 100$ m and the CFL value was set equal to
 6 0.4. The runs of the DE algorithm have been performed on a DELL PowerEdge R815 server with
 7 four 16-core, 2.5 GHz processors (64 cores total). The clock computational time for 1500
 8 generations was 781.3 min. Figure 3 displays the space-time evolution of the simulated speed,
 9 contrasted to the observations for the calibration day. Figure 4 depicts the measured and
 10 estimated speed dynamics for all detector locations around the congested area; as it can be
 11 observed, the real traffic conditions are well reproduced by the calibrated model, capturing with
 12 sufficient accuracy the onset of congestion with accurate timing and at the correct location, as
 13 observed in the real traffic data. The optimal model parameters and the minimum value of the
 14 cost function are given in Table 2.

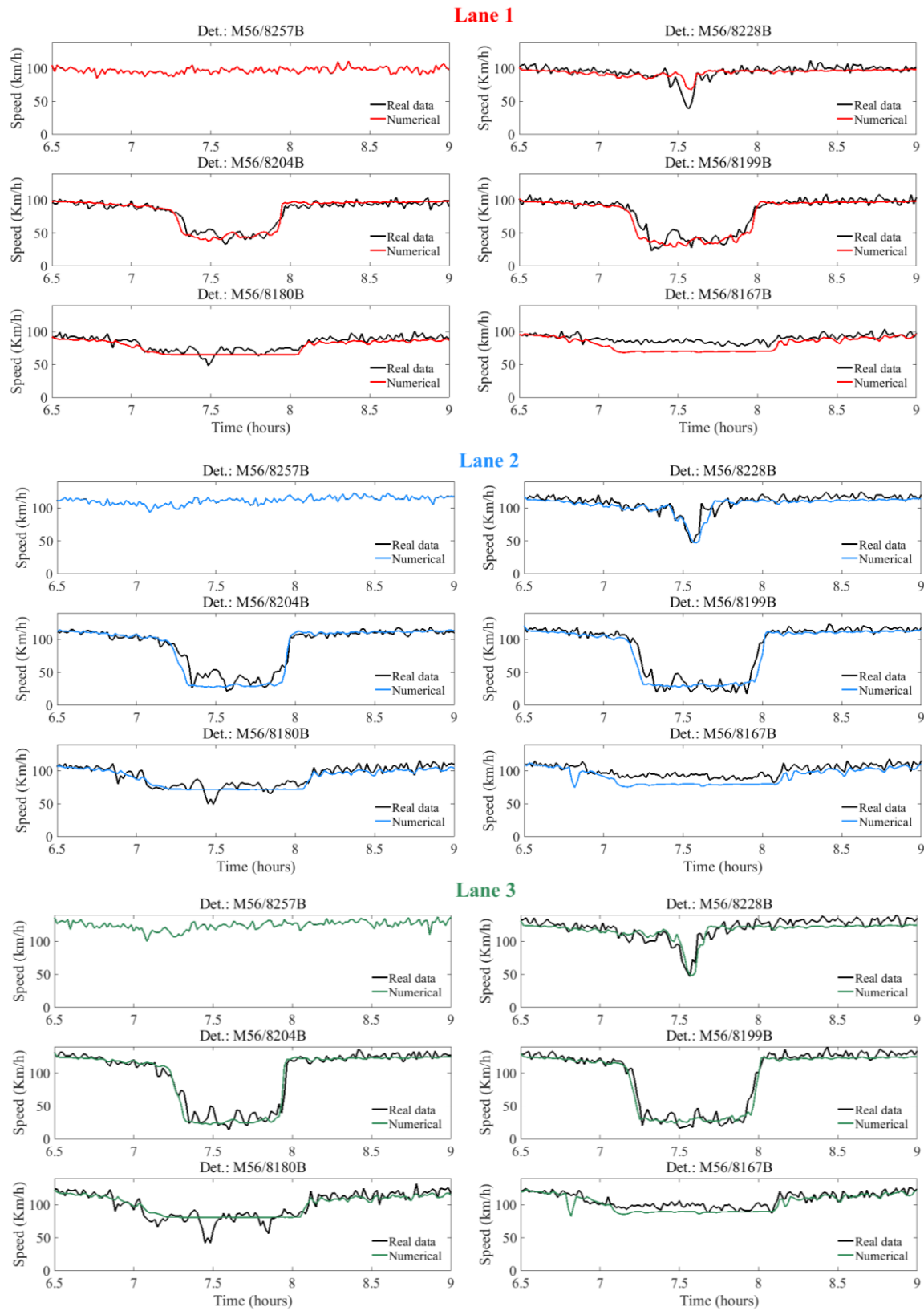
15
 16 **TABLE 2 Optimal model parameters and cost function value**

17

| Lanes | u_{max} | ρ_{max} | ρ_{cr} | T | γ | τ | A_0 | δA | $\delta \rho$ | v_f | ρ_p | $\left(\frac{u_{rmp}}{u_1}\right)$ | k_1^L | k_2^R | k_2^L | k_3^R |
|--------------------------------|----------------|------------------|-------------|-----|----------|--------|--------|------------|------------------|-------|----------|------------------------------------|---------------------------------|---------|---------|---------|
| | $\frac{km}{h}$ | $\frac{veh}{km}$ | | (s) | | (s) | - | - | $\frac{veh}{km}$ | - | - | - | $\frac{Events}{sec \cdot lane}$ | | | |
| Lane1 | 96 | 140 | 30 | 1.4 | 1.5 | 28 | 0.009 | 0.01 | 20 | 0.44 | 0.02 | 0.76 | 0.003 | 0.007 | 0.001 | 0.04 |
| Lane2 | 118 | 142 | 59 | 2 | 1.5 | 23 | 0.0065 | 0.032 | 10 | | | | | | | |
| Lane3 | 128 | 140 | 60 | 2 | 1.5 | 21 | 0.0064 | 0.032 | 14 | | | | | | | |
| Cost Function % : 0.029 | | | | | | | | | | | | | | | | |



20
 21 **FIGURE 3 Phase space speed dynamics for real measured speed (upper) and the model**
 22 **prediction (lower) for the calibration date.**

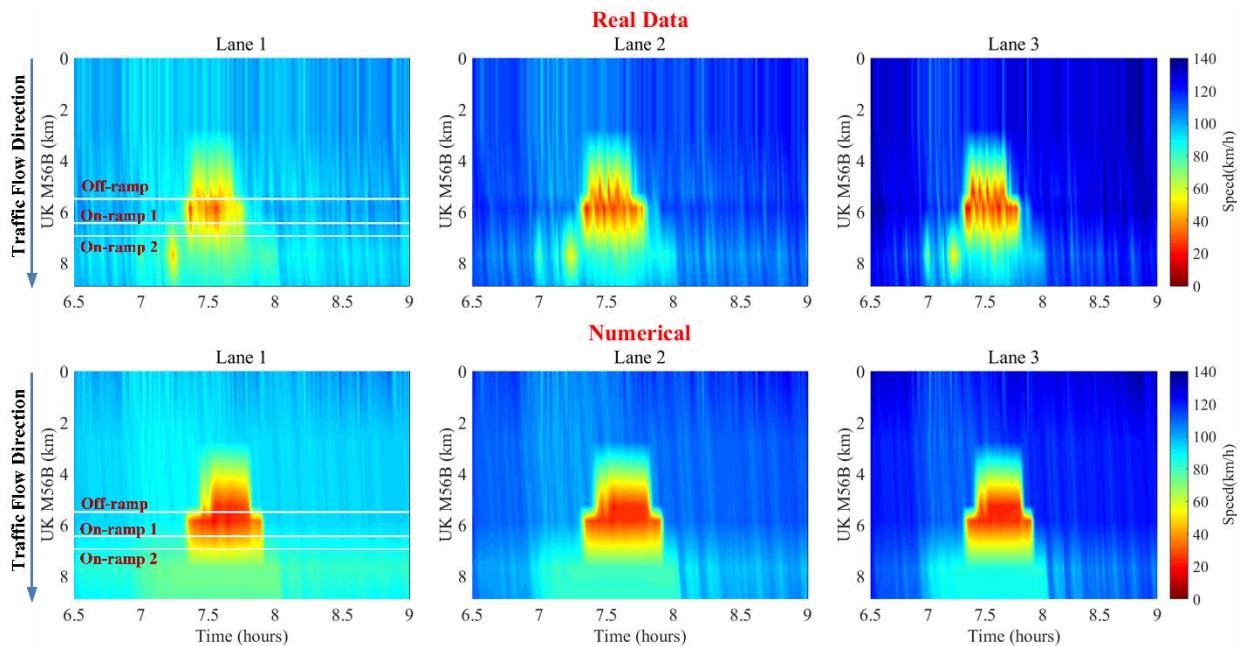


1
2

3 **FIGURE 4 Time-series of the real speed measurements (black) and the model prediction of**
4 **speed at various detector locations for the calibration day.**

1 **Validation results**

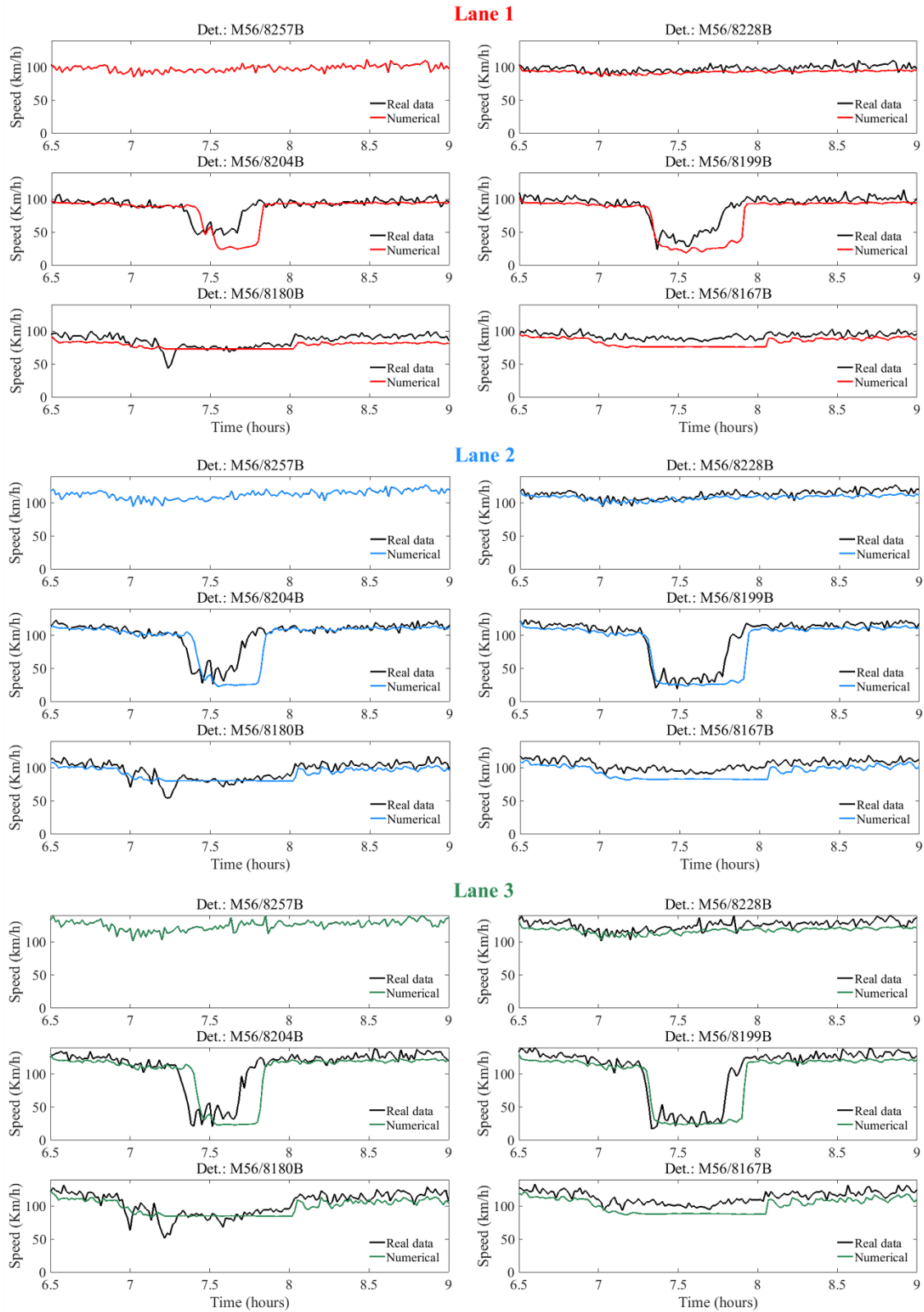
2 In order to assess the robustness of the produced calibrated parameters, the resulting multi-lane
 3 GKT model was validated using real traffic data in the same freeway stretch on a different day,
 4 which is the 24th of June 2014, using the optimal parameters of the previous calibration procedure.
 5 The validation results presented in Figure 5 and Figure 6, are seen to capture with sufficient
 6 accuracy the real traffic flow conditions in the particular freeway stretch, although not at the exact
 7 same level of accuracy as the calibrated ones. The cost function value for this validation procedure
 8 was 0.054 %. From the simulation results it can be observed that, although the value of the cost
 9 function is low, the simulation is not able to fully replicate all the flow fluctuations inside the
 10 congested region. To that end, other types of cost functions are currently under investigation.
 11 Nevertheless, the proposed model shows a good potential for simulating such traffic flow patterns
 12 in multi-lane highways.
 13



14 **FIGURE 5** Phase space speed dynamics for real measured speed (upper) and the model
 15 prediction (lower) for the validation date.
 16
 17

18 **CONCLUSIONS**

19 Within this study, a relatively new optimization tool, a parallel metamodel-assisted Differential
 20 Evolution (DE) algorithm, was employed for the automated calibration of a multi-lane (single-
 21 class) second-order macroscopic traffic flow model, based on the GKT one, for a specific
 22 freeway stretch using real traffic flow data. Following from the numerical results, the DE
 23 algorithm proved to be a promising and robust tool for the automated calibration of such a
 24 complicated multi-lane macroscopic model, having a relatively large number of (usually)
 25 counteracting calibration parameters. Actually, the obtained model predictions using the values
 26 of the optimal model parameters are consistent with the real measurements, showing that the
 27 developed multi-lane macroscopic model, with the specific hi-order discretization scheme, is
 28 able to reproduce with sufficient accuracy the prevailing traffic conditions; the robustness of the
 29 calibrated parameters is demonstrated through the validation process.
 30



1
2
3
4

FIGURE 6 Time-series of the real speed measurements (black) and the model prediction of speed at various detector locations for the validation day.

1 To the authors' best knowledge, this is the first time a calibration/validation procedure for such a
2 complicated multi-lane, second-order macroscopic traffic flow model, with such a large number
3 of calibration parameters, is reported.
4

5 **ACKNOWLEDGMENT**

6 This research was supported by TRAffic MANagement for the 21st century (TRAMAN21) ERC
7 Advanced Investigator Grand under the European Union's Seventh Framework Program
8 (FP/2007-20013). The authors are grateful to Highways England for providing access to the
9 MIDAS data.
10

11 **REFERENCES**

- 12 1. Hoogendoorn, S. and P. H. L. Bovy. State-of-the-art of Vehicular Traffic Flow
13 Modelling. In *Proceedings of the Institution of Mechanical Engineers, Part I:
14 Journal of Systems and Control Engineering*, Vol. 215, No. 4, 2001, pp. 283–303.
- 15 2. Richards, P. I. Shock Waves on the Highway. *Operations Research*, Vol. 4, No. 1,
16 1956, pp. 42–51.
- 17 3. Payne, H. J. Models of Freeway Traffic and Control. *Research Gate*, Vol. 28, 1971,
18 pp. 51–61.
- 19 4. Papageorgiou M. Some Remarks on Macroscopic Traffic Flow Modelling.
20 *Transportation Research Part A: Policy and Practice*, Vol. 32, No. 5, 1998, pp.
21 323–329.
- 22 5. Ni, D., J. D. Leonard II, A. Guin, and B. M. Williams. Systematic Approach for
23 Validating Traffic Simulation Models. In *Transportation Research Record: Journal
24 of the Transportation Research Board*, Vol. 1876, Transportation Research Board
25 of the National Academies, Washington, D.C., 2004, pp. 20–31.
- 26 6. Cremer, M., and M. Papageorgiou. Parameter Identification for a Traffic Flow Model.
27 *Automatica*, Vol. 17, No. 6, 1981, pp. 837–843.
- 28 7. Cremer, M. and J. Ludwig. A Fast Simulation Model for Traffic Flow on the Basis of
29 Boolean Operations. *Mathematics and Computers in Simulation*, Vol. 28, No. 4, 1986,
30 pp. 297–303.
- 31 8. Papageorgiou, M., J.-M. Blosseville, and H. Hadj-Salem. Macroscopic Modelling of
32 Traffic flow on the Boulevard Périphérique in Paris. *Transportation Research Part B
33 Methodological*, Vol. 23, No. 1, 1989, pp. 29–47.
- 34 9. Kotsialos, A., M. Papageorgiou, C. Diakaki, Y. Pavlis, and F. Middelham. Traffic Flow
35 Modeling of Large-scale Motorway Networks Using the Macroscopic Modeling Tool
36 METANET. *IEEE Transactions on Intelligent Transportation Systems*, Vol. 3, No. 4, 2002,
37 pp. 282–292.
- 38 10. Monamy, T., H. Hadj-Salem, and J.-P. Lebacque. A Macroscopic Node Model Related to
39 Capacity Drop. *Procedia - Social and Behavioral Sciences*, Vol. 54, 2012, pp. 1388–1396.
- 40 11. Ngoduy, D., S. Hoogendoorn, and H. Van Zuylen. Comparison of Numerical
41 Schemes for Macroscopic Traffic Flow Models. In *Transportation Research
42 Record: Journal of the Transportation Research Board*, Vol. 1876,
43 Transportation Research Board of the National Academies, Washington, D.C.,
44 2004, pp. 52–61.
- 45 12. Spiliopoulou, A., M. Kontorinaki, M. Papageorgiou, and P. Kopelias.
46 Macroscopic Traffic Flow Model Validation at Congested Freeway Off-ramp
47 Areas. *Transportation Research Part C Emerging Technologies*, Vol. 41, 2014,

- 1 pp. 18–29.
- 2 13. Poole, A. and A. Kotsialos. METANET Model Validation Using a Genetic
- 3 Algorithm. In *IFAC Proceedings Volumes (IFAC-PapersOnline)*, 2012, pp. 7-12.
- 4 14. Spiliopoulou, A., I. Papamichail, M. Papageorgiou, I. Tyrinopoulos, and J. Chrysoulakis.
- 5 Macroscopic Traffic Flow Model Calibration Using Different Optimization Algorithms.
- 6 *Transportation Research Procedia*, Vol. 6, 2015, pp. 144–157.
- 7 15. Ngoduy, D., and M. J. Maher. Calibration of Second-order Traffic Models Using
- 8 Continuous Cross Entropy Method. *Transportation Research Part C Emerging*
- 9 *Technologies*, Vol. 24, 2012, pp. 102–121.
- 10 16. Mudigonda, S., and K. Ozbay. Robust Calibration of Macroscopic Traffic Simulation
- 11 Models Using Stochastic Collocation. *Transportation Research Procedia*, Vol. 9, 2015,
- 12 pp. 1-20.
- 13 17. Gan, Q.-J., and W.-L. Jin. Validation of a Macroscopic Lane-Changing Model.
- 14 *Transportation Research Record: Journal of the Transportation Research Board*, No.
- 15 2391, Transportation Research Board of the National Academies, Washington, D.C.,
- 16 2013, pp. 113–123.
- 17 18. Delis, A. I., I. K. Nikolos and M. Papageorgiou. Macroscopic Modelling and Simulation
- 18 of Multi-lane Traffic. In *IEEE Conference on Intelligent Transportation Systems,*
- 19 *Proceedings, ITSC*, art. No. 7313449, 2015, pp. 2213-2218.
- 20 19. Delis, A. I., I. K. Nikolos, and M. Papageorgiou. High-resolution Numerical
- 21 Relaxation Approximations to Second-order Macroscopic Traffic Flow Models.
- 22 *Transportation Research Part C Emerging Technologies*, Vol. 44, 2014, pp. 318–
- 23 349.
- 24 20. Nikolos I. K. On the Use of Multiple Surrogates within a Differential Evolution
- 25 Procedure for High-lift Airfoil Design. *International Journal of Advanced*
- 26 *Intelligence Paradigms*, Vol. 5, No. 4, 2013, pp. 319–341.
- 27 21. Strofylas, G. A. and I. K. Nikolos. Reverse Engineering of a Wind Turbine Blade Surface
- 28 Using Differential Evolution. In *Proceedings of the 4th International Conference on Soft*
- 29 *Computing Technology in Civil, Structural and Environmental Engineering*, 2015.
- 30 22. Shvetsov, V., and D. Helbing. Macroscopic Dynamics of Multi-lane Traffic. *Physical*
- 31 *Review E - Statistical Physics, Plasmas, Fluids, and Related Interdisciplinary Topics*, Vol.
- 32 56, 1999, pp. 6328-6339.
- 33 23. Ngoduy, D., S. P. Hoogendoorn, and J. W. C. van Lint. Modeling Traffic Flow Operation
- 34 in Multilane and Multiclass Urban Networks. *Transportation Research Record: Journal*
- 35 *of the Transportation Research Board*, No. 1923, Transportation Research Board of the
- 36 National Academies, Washington, D.C., 2005, pp. 73–81.
- 37 24. Knoop, V.L., A. Duret, C. Buisson, and B. van Arem. Lane distribution of Traffic near
- 38 merging zones influence of variable speed limits. In *IEEE Conference on Intelligent*
- 39 *Transportation Systems, Proceedings, ITSC*, art. No. 5625034, 2010, pp. 485-490.
- 40 25. Highways Agency. *Motorway Incident Detection and Automatic Signaling (MIDAS)*
- 41 *Design Standard*. 1st edition, Bristol, UK, 2007.